HHS Public Access

Author manuscript

Angew Chem Int Ed Engl. Author manuscript; available in PMC 2024 March 25.

Published in final edited form as:

Angew Chem Int Ed Engl. 2023 December 04; 62(49): e202313880. doi:10.1002/anie.202313880.

High-Spin and Reactive Fe_{13} Cluster with Exposed Metal Sites

Anna G. Scott,
Division of Chemistry and Chemical Engineering, California Institute of Technology, Pasadena, CA 91125 (USA)

Diogo Alves Galico,
Department of Chemistry and Biomolecular Sciences, University of Ottawa, Ottawa, Ontario K1 N6 N5 (Canada)

Isabel Bogacz,
Molecular Biophysics and Integrated Bioimaging Division, Lawrence Berkeley National Laboratory Berkeley, CA 94720 (USA)

Paul H. Oyala,
Division of Chemistry and Chemical Engineering, California Institute of Technology, Pasadena, CA 91125 (USA)

Junko Yano[*],
Molecular Biophysics and Integrated Bioimaging Division, Lawrence Berkeley National Laboratory Berkeley, CA 94720 (USA)

Elizaveta A. Suturina[*],
Department of Chemistry, University of Bath, Claverton Down, Bath BA2 7AY (UK)

Muralee Murugesu[*],
Department of Chemistry and Biomolecular Sciences, University of Ottawa, Ottawa, Ontario K1 N6 N5 (Canada)

Theodor Agapie[*]
Division of Chemistry and Chemical Engineering, California Institute of Technology, Pasadena, CA 91125 (USA)

Abstract

Atomically defined large metal clusters have applications in new reaction development and preparation of materials with tailored properties. Expanding the synthetic toolbox for reactive high nuclearity metal complexes, we report a new class of Fe clusters, **Tp*$_4$W$_4$Fe$_{13}$S$_{12}$**, displaying a Fe_{13} core with M–M bonds that has precedent only in main group and late metal chemistry. M_{13} clusters with closed shell electron configurations can show significant stability and have been classified as superatoms. In contrast, **Tp*$_4$W$_4$Fe$_{13}$S$_{12}$** displays a large spin ground state of $S = 13$. This compound performs small molecule activations involving the transfer of up to 12 electrons resulting in significant cluster rearrangements.

[*] tagapie@caltech.edu, m.murugesu@uottawa.ca, jyano@lbl.gov, e.suturina@bath.ac.uk.

Conflict of Interest

The authors declare no conflict of interest.

Keywords

High-Spin; Iron-Sulfur Clusters; Magnetic Properties; Small Molecule Activation; Metal-Metal Interactions

Isolable transition metal-only high nuclearity clusters of well-defined atomic composition and structure are of interest for understanding nanoparticle growth processes and electronic structures, new optical and magnetic properties, designing new materials with tailored properties, tuning reactivity, and modeling heterogeneous catalysts.[1–8] Towards such applications, larger transition metal-only clusters displaying M–M interactions, without supporting interstitial bridging anionic ligands have been prepared for late transition metals, most commonly noble metals, although examples are known for first row transition metals such as Cu and Ni.[5,9–21] Isolation of some of these clusters is proposed to be facilitated by a closed shell electronic configuration that imparts particular stability within the superatom model.[22,23] However, while the structure of numerous large clusters has been determined using single-crystal X-ray diffraction (SC-XRD), use of such clusters to gain atomic level insight into reactivity on the surface of clusters has typically been hindered by a saturated coordination sphere and the propensity of complex clusters to fragment into smaller species.[23,24]

Toward developing new reactivity, synthetic protocols for larger clusters with open coordination sites for reaction chemistry and a greater number of metal-metal interactions are desirable.[25,26] Synthetic procedures for clusters of transition metals typically use metal salt precursors in combination with reducing agents and organic ligands.[1,7,9,27–29] Modification of known clusters has been demonstrated as a complementary route to new complexes.[10,12,30] Assembly of tetranuclear iron-sulfur clusters into oligomers upon halide abstraction or reduction provides precedent for employing small clusters to generate higher complexity structures, though typically containing interstitial bridges.[31,32] Herein, we employ a tetranuclear precursor **$[Et_4N]_2[Tp^*WFe_3S_3(u_3\text{-}Cl)Cl_3]$**[33] ($Et_4N$=tetraethylammonium, Tp*=tris(3,5-dimethyl-1-pyrazolyl)borate) as a building unit to a more complex cluster, **$Tp^*_4W_4Fe_{13}S_{12}$**, with an unprecedented Fe_{13} core. **$Tp^*_4W_4Fe_{13}S_{12}$**, a cluster with high-spin ground state, displays open coordination sites and is reactive, yet sufficiently stabilized to allow the isolation of small molecule activation products including complexes with surface nitride, imide, and sulfide groups.

Toward lower oxidation state high nuclearity clusters for reductive reactivity, we employed precursors anchored by the robust Tp^*WS_3 unit.[34] Taking advantage of the lability of the chloride ligands in the presence of a halide abstracting reagent in comparison to the thiolate, phosphine, carbene, sulfide, or nitride ligands of previously reported clusters,[31,33] we previously developed reduction chemistry starting from **$[Et_4N]_2[Tp^*WFe_3S_3(\mu_3\text{-}Cl)Cl_3]$**[33] (Figure 1A,) to access $Tp^*WFe_3S_3$ complexes supported by carbene ligands (L) with Fe_3 open faces.[35] To generate higher nuclearity clusters, reduction was performed in the absence of additional supporting ligands L that could trap small metal clusters.

Treatment of **$[Et_4N]_2[Tp^*WFe_3S_3(\mu_3\text{-}Cl)Cl_3]$** with reductant and halogen abstracting reagent results in a cluster with the overall chemical formula **$Tp^*_4W_4Fe_{13}S_{12}$** as determined

by SC-XRD (Figure 1A). **Tp*$_4$W$_4$Fe$_{13}$S$_{12}$** consists of four Tp*WS_3 units tetrahedrally arranged (Figure 1D) around a pseudo-icosahedral Fe_{12} core with an additional Fe atom bound in the center.[36] The Fe–Fe distances are between 2.395(2) and 2.771(2) Å (Table S1), within the range of metal-metal bonds for molecular Fe complexes.[37,38] The W–S distances match the parameters observed for reduced Tp*WFe_3S_3 clusters supported by N-heterocyclic carbene ligands at Fe.[35] The Fe–S bonds show a significant lengthening relative to the precursor, consistent with reduction at Fe.[39] Overall, the 17 metal centers carry a 28+ charge, M_{17}^{28+}. There are four open Fe_3 faces, each with three surrounding bridging sulfides that create a cavity around these potential binding sites (Figure 1C, S2).

The icosahedral metal cluster motif is known for transition metals past group 8.[10,11,41] Lower symmetry reduced clusters of group 8 metals, Ru_{10} and Os_{20},[42,43] have been reported, but are coordinately saturated with CO ligands. Icosahedral M_{13} clusters of main group and later transition metals, including $[Al_{13}]^-$, $[Au_{13}]^{5+}$, and $[Cu_{13}]^{5+}$, have been reported to be particularly robust and are described as metallic superatoms due to their closed shell electronic structure in the Jellium model and full shell of 12 atoms around the central metal.[1,10,44] To probe the open shell nature of **Tp*$_4$W$_4$Fe$_{13}$S$_{12}$** direct current (dc) susceptibility measurements were performed on a polycrystalline sample restrained in grease to prevent torquing (see SI). At room temperature, a χT value of 98.39 cm^3 K mol^{-1} is observed (Figure 1E), which suggests the presence of $S = 13$ ground state open shell system. It is reasonable to assume all the spins within the clusters are strongly coupled even at room temperature, given the metal-metal bonded core within the cluster. Upon reducing the temperature, the χT product slightly increases to 106.67 cm^3 K mol^{-1} at 80 K. Such behavior was also previously seen for the hexanuclear metal-metal bonded Fe clusters.[45–47] The χT product remains relatively constant down to 10 K; thereafter it decreases rapidly to reach a minimum value of 58.89 cm^3 K mol^{-1} at 1.8 K. The low temperature behavior is likely due to zero-field splitting. To probe further, magnetization measurements at variable fields (0–7 T) in the temperature range of 2–9 K were performed on **Tp*$_4$W$_4$Fe$_{13}$S$_{12}$**. Fitting of the data using PHI software[40] afforded a ground spin state of $S = 13$ ($D = -2.1$ cm^{-1}, $E/D = 0.24$, and $g = 2.16$, Figure 1E and S4). A continuous-wave electron paramagnetic resonance (CW-EPR) study of **Tp*$_4$W$_4$Fe$_{13}$S$_{12}$** reveals transitions in both parallel and perpendicular modes and fitting of the data using $S = 13$ yielded $D = -0.2$ cm^{-1}, $E/D = 0.013$, and $g = 1.9$ (Figure S8). These results clearly set this system apart from the previously reported closed shell metallic superatoms.

To address electron distribution within the cluster, X-ray absorption near edge spectroscopy (XANES) experiments were performed on **[Et$_4$N]$_2$[Tp*WFe$_3$S$_3$(μ$_3$-Cl)Cl$_3$]** and **Tp*$_4$W$_4$Fe$_{13}$S$_{12}$** to probe the W L_2 and L_3 edge, considering that the coordination sphere of W is maintained across these clusters (Figures 1B, S7). Peak centers remain at 10214.2 eV for both clusters, while there is a less than 0.1 eV white line shift for L_2 and no shift for L_3. Assuming an oxidation state for **[Et$_4$N]$_2$[Tp*WFe$_3$S$_3$(μ$_3$-Cl)Cl$_3$]** as W(III),[48,49] a similar effective charge is maintained for **Tp*$_4$W$_4$Fe$_{13}$S$_{12}$** according to the XANES data, although further studies are needed to conclusively assign the oxidation state.[50,51] Given this tentative W(III) assignment, the formal charge distribution on Fe is $[Fe_{13}]^{16+}$, placing 88 electrons in Fe *d*-based molecular orbitals. With only three weak

field ligands coordinated to each outer Fe center, low d-d splitting is expected. Within the *d*-based molecular orbital manifold for the Fe–Fe and Fe–S interactions, the highest spin state corresponds to 42 unpaired electrons for $[Fe_{13}]^{16+}$. A sufficiently large orbital splitting resulting in an intermediate spin orbital population in combination with antiferromagnetic interactions with the four W centers[52,53] could bring the spin value of **Tp*$_4$W$_4$Fe$_{13}$S$_{12}$** in the range estimated from the magnetization data.

Quantum chemistry calculations of different spin states (from $S = 1$ to $S = 37$) at BP86/def2-SVP level of theory done using the XRD structure of **Tp*$_4$W$_4$Fe$_{13}$S$_{12}$** suggest that the lowest energy state has a considerably high total spin of $S = 16$ (Figure 2, Table S3); the experimentally determined $S = 13$, however, is close in energy. Fitting of the magnetism and CW-EPR data using ground spin states of $S = 13$ or 16 yielded satisfactory fits (Figures S4–S6, S8). These results suggest that the spin states of similar energies are plausible ground states for this complex. Computationally, in the $S = 16$ state, the Mulliken spin population on W is −0.8/−0.9 suggesting that each tungsten carries one unpaired electron with the spin antiparallel to the spin of Fe_{13} core. All spins of the Fe centers are aligned with each other, and the spin population is 2.7/2.8 on the peripheral ions while the Fe center in the middle of the cluster has a spin population of 1.5. The magnetic moment per Fe atom is close to the calculated values for neutral and mono cationic/anionic Fe clusters of various sizes despite much smaller number of electrons in the formally $[Fe_{13}]^{16+}$ core.[54]

Clusters with notably high-spin ground states are typically generated from higher nuclearity clusters with bridging ligands, such as oxides, that facilitate superexchange pathways for spin coupling.[55–58] However, these weak interactions are overcome at high temperatures. Stronger coupling can be achieved through a molecular orbital manifold in complexes with intermediate strength metal-metal interactions resulting in moderate splitting of the *d*-based orbitals, where the cluster is conceptually analogous to a high-spin single metal complex.[45,47,49,60] Overall, **Tp*$_4$W$_4$Fe$_{13}$S$_{12}$** demonstrates a strategy to achieve high-spin states through high nuclearity metallic cores terminated with weak field bridging sulfide ligands.

Several aspects of **Tp*$_4$W$_4$Fe$_{13}$S$_{12}$** suggest potential for reactivity, including a relatively reduced redox state, open coordination sites, a high spin, and metal-metal bonds. The open, coordinately unsaturated Fe_3 faces are reminiscent of triangular motifs known to undergo small molecule activations for M_3 clusters,[37,61,62] including nitrogen atom and nitrene transfer chemistry in up to four electron redox processes.[37,63–66] Such studies have shown that metal-metal interactions can allow for multi-electron redox chemistry without metal centers in particularly low oxidation states. **Tp*$_4$W$_4$Fe$_{13}$S$_{12}$** has four of these surface Fe_3 structural motifs as well as the additional redox active central Fe atom and distal W centers. Considering that heterogeneous iron catalysts are employed in the Haber-Bosch process and insight into the bonding of proposed intermediates of N_2 reduction to multimetallic sites is limited,[67,68] we targeted reactions with nitrogenous ligands. Reaction of **Tp*$_4$W$_4$Fe$_{13}$S$_{12}$** with four equivalents of trimethylsilylazide (N_3SiMe_3) results in the transfer of four nitride atoms (Figure 3) to generate **Tp*$_4$W$_4$Fe$_{13}$S$_{12}$N$_4$** in an overall 12 electron process, a remarkable number for a single molecule. The Fe_{13} core has been converted from a centered icosahedron to a centered cuboctahedron (Figure 3, 4).[10,44] Despite the substantial reorganization of the Fe_{13} core and the formal transfer of 12

electrons, the Fe–Fe distances (2.568(2)–2.737(2) Å, Table S1) remain within the range of the starting material suggesting a propensity to maintain metal-metal interactions.[36] The W–S bond lengths shorten slightly, to an average length of 2.331(9) Å, suggesting partial oxidation at W. DFT studies of the relative stability of gas phase metal clusters without supporting ligands[69] indicate that the metal oxidation states impact the energies of various cluster geometries, of potential consequence here given the redox changes between M_{17}^{28+} and M_{17}^{40+}. Comparison of **Tp*$_4$W$_4$Fe$_{13}$S$_{12}$** and **Tp*$_4$W$_4$Fe$_{13}$S$_{12}$N$_4$** demonstrates that cluster reorganization remains possible in the presence of surface ligands, where the energetics of metal-ligand interactions on geometry must be taken into account. For example, whereas the sulfides of the Tp*WS$_3$ fragments each bind trigonal Fe$_3$ faces in **Tp*$_4$W$_4$Fe$_{13}$S$_{12}$**, they coordinate to Fe–Fe edges of Fe$_4$ squares in **Tp*$_4$W$_4$Fe$_{13}$S$_{12}$N$_4$** (Figure S9). Compared to **Tp*$_4$W$_4$Fe$_{13}$S$_{12}$**, **Tp*$_4$W$_4$Fe$_{13}$S$_{12}$N$_4$** exhibits a white line shift of 1.5 eV for the W L_2 edge and 1.0 eV for the W L_3 edge (Figure 1B, S7). While this indicates a change in charge density at W, which is remote from the site of reaction chemistry at Fe, further studies are needed to assign formal oxidation state changes.

To gain access to an imide analog of **Tp*$_4$W$_4$Fe$_{13}$S$_{12}$N$_4$** for comparison, reactions with phenyl azide (PhN$_3$) were performed. Treatment of **Tp*$_4$W$_4$Fe$_{13}$S$_{12}$** with three equivalents of PhN$_3$ resulted in the isolation of the tris-imide species **Tp*$_4$W$_4$Fe$_{13}$S$_{12}$(NPh)$_3$**.[36] Again, all of the atoms of the cluster precursor are maintained, and the geometry is altered toward a centered cuboctahedral geometry, but with substantial distortions (Figure 3, 4).

Despite the redox state and Fe$_{13}$ structure being between those of **Tp*$_4$W$_4$Fe$_{13}$S$_{12}$** and **Tp*$_4$W$_4$Fe$_{13}$S$_{12}$N$_4$**, **Tp*$_4$W$_4$Fe$_{13}$S$_{12}$(NPh)$_3$** displays Fe–Fe distances that are longer than both (up to 2.941(5) Å compared to 2.737(2) and 2.771(2) Å, respectively). This observation indicates that the M–M distances are not directly predicated by the redox state of the metal. In fact, the cluster of intermediate oxidation state has the longest M–M distance.

To further explore the impact of the group transferred on the cluster structure, installation of sulfide was targeted, as a ligand isolobal to both nitride and imide. **Tp*$_4$W$_4$Fe$_{13}$S$_{12}$** reacts with two equivalents of triphenylphosphine sulfide (SPPh$_3$) to form **Tp*$_4$W$_4$Fe$_{13}$S$_{14}$** (Figure 3), as observed by SC-XRD and the byproduct PPh$_3$ (^{31}P NMR spectroscopy, Figure S11).[36] Two sulfur atoms have been transferred, in contrast to three and four for the reactions with PhN$_3$ and Me$_3$SiN$_3$, respectively, in a four electron redox process. The Fe$_{13}$ core of the product has lower symmetry and becomes distorted from an icosahedron such that two of the Fe–Fe distances increase to greater than 3 Å (Figure 3 and 4).

Analysis of the multiiron layers below an open triangular Fe$_3$ face in the precursor (**Tp*$_4$W$_4$Fe$_{13}$S$_{12}$**) versus a ligand coordinated Fe$_3$ face in each of the group transfer cluster products shows substantial Fe atom shifts (Figure 4). Notably, the most pronounced variation of Fe–Fe distances within one cluster were observed in the cases where fewer groups and electrons were transferred.

In summary, we report a synthetic strategy for the synthesis of metallic Fe$_{13}$ clusters upon reduction of a tetranuclear precursor, **[Et$_4$N]$_2$[Tp*WFe$_3$S$_3$(μ$_3$-Cl)Cl$_3$]**. The atomically precise characterization of **Tp*$_4$W$_4$Fe$_{13}$S$_{12}$**, **Tp*$_4$W$_4$Fe$_{13}$S$_{12}$N$_4$**, **Tp*$_4$W$_4$Fe$_{13}$S$_{12}$(NPh)$_3$**,

and **$Tp^*_4W_4Fe_{13}S_{14}$** demonstrates that large clusters can maintain the metallic core while performing well-defined multi-electron multiple group transfer chemistry with overall redox changes of 4 to 12 electrons. **$Tp^*_4W_4Fe_{13}S_{12}$** shows a notably high magnetic moment at room temperature for metallic clusters, highlighting the potential of this type of coordination compound for magnetic materials applications. The structural variation observed with the present clusters shows the ability of multimetallic systems to accommodate the bonding requirements of large redox and ligand changes. The propensity for surface rearrangement demonstrated with the transfer of nitrogen, nitrene, and sulfur ligands can serve as a tool for new reactive cluster design. The availability of clusters displaying the $Tp^*WM_3S_3$ motif for other transition metals[70] provides a starting point to a broader range of large metallic clusters related to those reported here.

Supplementary Material

Refer to Web version on PubMed Central for supplementary material.

Acknowledgements

We are grateful to the National Institutes of Health (R01-GM102687B to T.A.) and the National Science Foundation (Graduate Research Fellowships Program to A.G.S.) for funding, the Beckman Institute and the Dow Next Generation Grant for instrumentation support, Michael Takase and Lawrence Henling for assistance with crystallography. Part of this work (XAS data collection) was carried out at the Stanford Synchrotron Radiation Lightsource, SLAC National Accelerator Laboratory, which is supported by the U.S. Department of Energy, Office of Science, Office of Basic Energy Sciences under Contract No. DE-AC02-76SF00515. XAS studies were performed with support of the NIH GM110501 (J.Y.). EAS gratefully acknowledges the University of Bath's Research Computing Group (doi.org/10.15125/b6cd-s854) for their support in this work.

Data Availability Statement

The data that support the findings of this study are available in the supplementary material of this article.

References

[1]. Doud EA, Voevodin A, Hochuli TJ, Champsaur AM, Nuckolls C, Roy X, Nat. Rev. Mater. 2020, 5, 371–387.

[2]. Claridge SA, Castleman AW, Khanna SN, Murray CB, Sen A, Weiss PS, ACS Nano 2009, 3, 244–255. [PubMed: 19236057]

[3]. Yan N, Yuan Y, Dyson PJ, Dalton Trans. 2013, 42, 13294–13304. [PubMed: 23770799]

[4]. Reiss G, Hütten A, Nat. Mater. 2005, 4, 725–726. [PubMed: 16195762]

[5]. Du Y, Sheng H, Astruc D, Zhu M, Chem. Rev. 2020, 120,526–622. [PubMed: 30901198]

[6]. Robertson DD, Personick ML, Chem. Mater. 2019, 31, 1121–1141.

[7]. Jin R, Li G, Sharma S, Li Y, Du X, Chem. Rev. 2021, 121, 567–648. [PubMed: 32941029]

[8]. Liu L, Corma A, Chem. Rev. 2018, 118, 4981–5079. [PubMed: 29658707]

[9]. Nguyen T-AD, Jones ZR, Goldsmith BR, Buratto WR, Wu G, Scott SL, Hayton TW, J. Am. Chem. Soc. 2015, 137, 13319–13324. [PubMed: 26422670]

[10]. Chakrahari KK, Liao J-H, Kahlal S, Liu Y-C, Chiang M-H, Saillard J-Y, Liu CW, Angew. Chem. Int. Ed. 2016, 55, 14704–14708.

[11]. Dhayal RS, Liao J-H, Wang X, Liu Y-C, Chiang M-H, Kahlal S, Saillard J-Y, Liu CW, Angew. Chem. Int. Ed. 2015, 54, 13604–13608.

[12]. Nguyen T-AD, Jones ZR, Leto DF, Wu G, Scott SL, Hayton TW, Chem. Mater. 2016, 28, 8385–8390.

[13]. Sugiuchi M, Shichibu Y, Nakanishi T, Hasegawa Y, Konishi K, Chem. Commun. 2015, 51, 13519–13522.

[14]. Touchton AJ, Wu G, Hayton TW, Inorg. Chem. 2021, 60, 17586–17592. [PubMed: 34762406]

[15]. Brennan JG, Siegrist T, Kwon YU, Stuczynski SM, Steigerwald ML, J. Am. Chem. Soc. 1992, 114, 10334–10338.

[16]. Fenske D, Krautscheid H, Müller M, Angew. Chem. Int. Ed. 1992, 31, 321–323.

[17]. Qian H, Zhu M, Wu Z, Jin R, Acc. Chem. Res. 2012, 45,1470–1479. [PubMed: 22720781]

[18]. Yang H, Wang Y, Zheng N, Nanoscale 2013, 5, 2674–2677. [PubMed: 23467729]

[19]. Desireddy A, Conn BE, Guo J, Yoon B, Barnett RN, Monahan BM, Kirschbaum K, Griffith WP, Whetten RL, Landman U, Bigioni TP, Nature 2013, 501, 399–402. [PubMed: 24005327]

[20]. Erickson JD, Mednikov EG, Ivanov SA, Dahl LF, Am J. Chem. Soc. 2016, 138, 1502–1505.

[21]. Chini P, J. Organomet. Chem. 1980, 200, 37–61.

[22]. Reber AC, Khanna SN, Acc. Chem. Res. 201, 50, 255–263.

[23]. Walter M, Akola J, Lopez-Acevedo O, Jadzinsky PD, Calero G, Ackerson CJ, Whetten RL, Grönbeck H, Häkkinen H, Proc. Natl. Acad. Sci. USA 2008, 105, 9157–9162. [PubMed: 18599443]

[24]. Eremin DB, Ananikov VP, Coord. Chem. Rev. 201, 346,2–19.

[25]. Takano S, Tsukuda T, J. Am. Chem. Soc. 2021, 143, 1683–1698. [PubMed: 33481579]

[26]. Yang H, Wang Y, Lei J, Shi L, Wu X, Mäkinen V, Lin S, Tang Z, He J, Häkkinen H, Zheng L, Zheng N, J. Am. Chem. Soc. 2013, 135, 9568–9571. [PubMed: 23789787]

[27]. Si W-D, Li Y-Z, Zhang S-S, Wang S, Feng L, Gao Z-Y, Tung C-H, Sun D, ACS Nano 2021, 15, 16019–16029. [PubMed: 34592104]

[28]. Sun C, Mammen N, Kaappa S, Yuan P, Deng G, Zhao C, Yan J, Malola S, Honkala K, Häkkinen H, Teo BK, Zheng N, ACS Nano 2019, 13, 5975–5986. [PubMed: 31067029]

[29]. Zhu M, Lanni E, Garg N, Bier ME, Jin R, J. Am. Chem. Soc. 2008, 130, 1138–1139. [PubMed: 18183983]

[30]. Ito E, Takano S, Nakamura T, Tsukuda T, Angew. Chem. Int. Ed. 2021, 60, 645–649.

[31]. Lee SC, Lo W, Holm R, Chem. Rev. 2014, 114, 3579–3600. [PubMed: 24410527]

[32]. Xu G, Zhou J, Wang Z, Holm RH, Chen X-D, Angew. Chem. Int. Ed. 2019, 58, 16469–16473.

[33]. Xu G, Wang Z, Ling R, Zhou J, Chen X-D, Holm RH, Proc. Natl. Acad. Sci. USA 2018, 115, 5089–5092. [PubMed: 29654147]

[34]. Zheng B, Chen X-D, Zheng S-L, Holm RH, J. Am. Chem. Soc. 2012, 134, 6479–6490. [PubMed: 22424175]

[35]. Le LNV, Bailey GA, Scott AG, Agapie T, Proc. Natl. Acad. Sci. USA 2021, 118, e2109241118. [PubMed: 34857636]

[36]. Deposition numbers 2128366 (for Tp*4W4Fe13S12), 2128365 (for Tp*4W4Fe13S12N4), 2128364 (for Tp*4W4Fe13S12(NPh)3), and 2128367 (for Tp*4W4Fe13S14) contain the supplementary crystallographic data for this paper. These data are provided free of charge by the joint Cambridge Crystallographic Data Centre and Fachinformationszentrum Karlsruhe Access Structures service.

[37]. Powers TM, Betley TA, J. Am. Chem. Soc. 2013, 135,12289–12296. [PubMed: 23865953]

[38]. Pushkarevsky NA, Konchenko SN, Zabel M, Bodensteiner M, Scheer M, Dalton Trans. 2011, 40, 2067–2074. [PubMed: 21258730]

[39]. Majumdar A, Holm R, Inorg. Chem. 2011, 50, 11242–11251. [PubMed: 21985054]

[40]. Chilton NF, Anderson RP, Turner LD, Soncini A, Murray KS, J. Comput. Chem. 2013, 34, 1164–1175. [PubMed: 23386394]

[41]. Laupp M, Strähle J, Angew. Chem. Int. Ed. 1994, 33, 207–209.

[42]. Bailey PJ, Beswick MA, Johnson BFG, Lewis J, Raithby PR, de Arellano MCR, J. Chem. Soc. Dalton Trans. 1992, 3159–3160.

[43]. Gade LH, Johnson BFG, Lewis J, McPartlin M, Powell HR, Raithby PR, Wong W-T, J. Chem. Soc. Dalton Trans. 1994, 521–532.

[44]. Roduner E, Phys. Chem. Chem. Phys. 2018, 20, 23812–23826. [PubMed: 30215081]

[45]. Sánchez RH, Betley TA, J. Am. Chem. Soc. 2018, 140,16792–16806. [PubMed: 30403845]

[46]. Nehrkorn J, Greer SM, Malbrecht BJ, Anderton KJ, Aliabadi A, Krzystek J, Schnegg A, Holldack K, Herrmann C, Betley TA, Stoll S, Hill S, Inorg. Chem. 2021, 60, 4610–4622. [PubMed: 33683105]

[47]. Hernández Sánchez R, Betley TA, J. Am. Chem. Soc. 2015, 137, 13949–13956. [PubMed: 26440452]

[48]. Hong D, Zhang Y, Holm RH, Inorg. Chim. Acta 2005, 358, 2303–2311.

[49]. Hauser C, Bill E, Holm RH, Inorg. Chem. 2002, 41, 1615–1624. [PubMed: 11896732]

[50]. Kowalska JK, Hahn AW, Albers A, Schiewer CE, Bjornsson R, Lima FA, Meyer F, DeBeer S, Inorg. Chem. 2016, 55, 4485–4497. [PubMed: 27097289]

[51]. Jayarathne U, Chandrasekaran P, Greene AF, Mague JT, DeBeer S, Lancaster KM, Sproules S, Donahue JP, Inorg.Chem. 2014, 53, 8230–8241. [PubMed: 25068843]

[52]. Bjornsson R, Lima FA, Spatzal T, Weyhermüller T, Glatzel P, Bill E, Einsle O, Neese F, DeBeer S, Chem. Sci. 2014, 5, 3096–3103.

[53]. Bigness A, Vaddypally S, Zdilla MJ, Mendoza-Cortes JL, Coord. Chem. Rev. 2022, 450, 214168.

[54]. Gutsev GL, Weatherford CA, Jena P, Johnson E, Ramachandran BR, J. Phys. Chem. A 2012, 116, 10218–10228. [PubMed: 23039843]

[55]. Ako AM, Hewitt IJ, Mereacre V, Clérac R, Wernsdorfer W, Anson CE, Powell AK, Angew. Chem. Int. Ed. 2006, 45, 4926–4929.

[56]. Qin L, Zhang H-L, Zhai Y-Q, Nojiri H, Schröder C, Zheng Y-Z, iScience 2021, 24, 102350. [PubMed: 33898945]

[57]. Manoli M, Alexandrou S, Pham L, Lorusso G, Wernsdorfer W, Evangelisti M, Christou G, Tasiopoulos AJ, Angew. Chem. Int. Ed. 2016, 55, 679–684.

[58]. Kang S, Zheng H, Liu T, Hamachi K, Kanegawa S, Sugimoto K, Shiota Y, Hayami S, Mito M, Nakamura T, Nakano M, Baker ML, Nojiri H, Yoshizawa K, Duan C, Sato O, Nat. Commun. 2015, 6, 5955. [PubMed: 25562786]

[59]. Greer SM, Gramigna KM, Thomas CM, Stoian SA, Hill S, Inorg. Chem. 2020, 59, 18141–18155. [PubMed: 33253552]

[60]. Chipman JA, Berry JF, Chem. Rev. 2020, 120, 2409–2447. [PubMed: 32045223]

[61]. Ermert DM, Gordon JB, Abboud KA, Murray LJ, Inorg. Chem. 2015, 54, 9282–9289. [PubMed: 26052673]

[62]. Wucherer EJ, Tasi M, Hansert B, Powell AK, Garland MT, Halet JF, Saillard JY, Vahrenkamp H, Inorg. Chem. 1989, 28, 3564–3572.

[63]. Bartholomew AK, Juda CE, Nessralla JN, Lin B, Wang SG, Chen Y-S, Betley TA, Angew. Chem. Int. Ed. 2019, 58, 5687–5691.

[64]. Dunn PL, Chatterjee S, MacMillan SN, Pearce AJ, Lancaster KM, Tonks IA, Inorg. Chem. 2019, 58, 11762–11772. [PubMed: 31436979]

[65]. Li Y, Wong W-T, Coord. Chem. Rev. 2003, 243, 191–212.

[66]. Sappa E, Milone L, J. Organomet. Chem. 19 3, 61, 383–388.

[67]. Fuller J, Fortunelli A, Iii WAG, An Q, Phys. Chem. Chem. Phys. 2019, 21, 11444–11454. [PubMed: 31112166]

[68]. Qian J, An Q, Fortunelli A, Nielsen RJ, Goddard WA, J. Am. Chem. Soc. 2018, 140, 6288–6297. [PubMed: 29701965]

[69]. Piotrowski MJ, Piquini P, Da Silva JLF, Phys. Rev. B 2010, 81, 155446.

[70]. Wang J, Sun Z-R, Deng L, Wei Z-H, Zhang W-H, Zhang Y, Lang J-P, Inorg. Chem. 200, 46, 11381–11389.

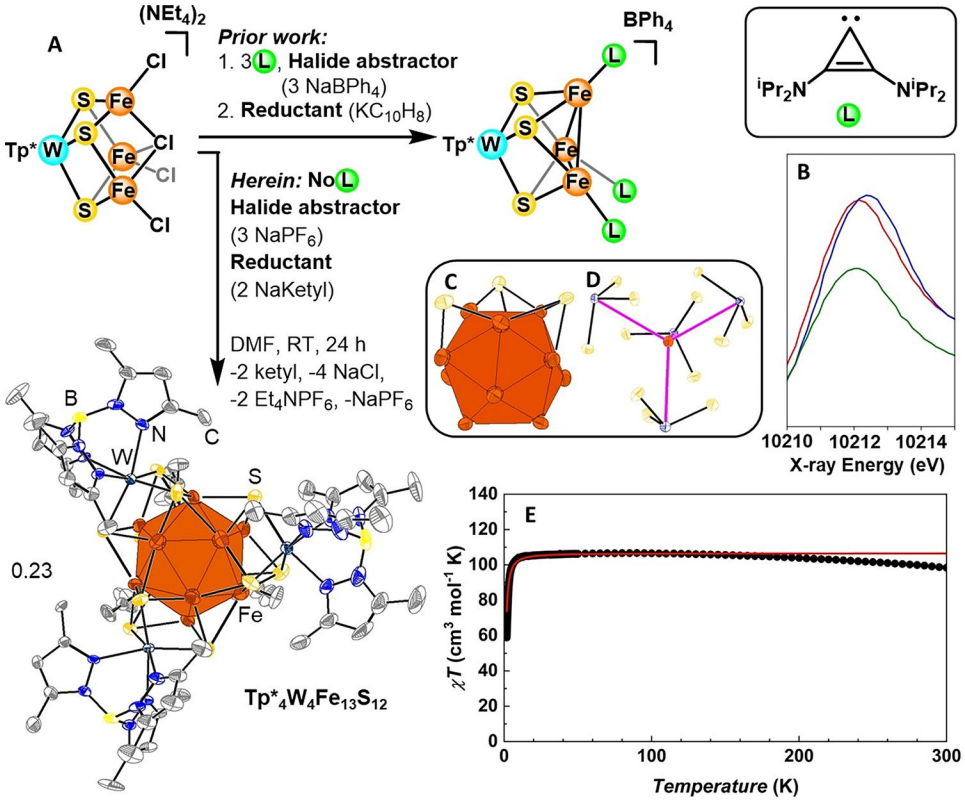

Figure 1.

(A) Synthesis of **$Tp^*_4W_4Fe_{13}S_{12}$**. Solvent and hydrogen atoms omitted for clarity and ellipsoids plotted at the 50% probability level. (B) W L_3 XANES data for **$[Et_4N]_2[Tp^*WFe_3S_3(\mu_3\text{-}Cl)Cl_3]$** (green), **$Tp^*_4W_4Fe_{13}S_{12}$** (red), and **$Tp^*_4W_4Fe_{13}S_{12}N_4$** (blue). (C) Fe_{13} core highlighting one Fe_3S_3 cavity motif. (D) Tetrahedral arrangement of 4 WS_3 units around the central Fe atom of the Fe_{13} core. (E) Direct current variable temperature magnetic susceptibility measurement for **$Tp^*_4W_4Fe_{13}S_{12}$** (black circles) collected from 1.8 to 300 K, after diamagnetic correction. Red line corresponds to the best fitting using PHI software ($S = 13$, $D = -2.1$ cm^{-1}, $E/D = 0.24$, and $g = 2.16$).[40]

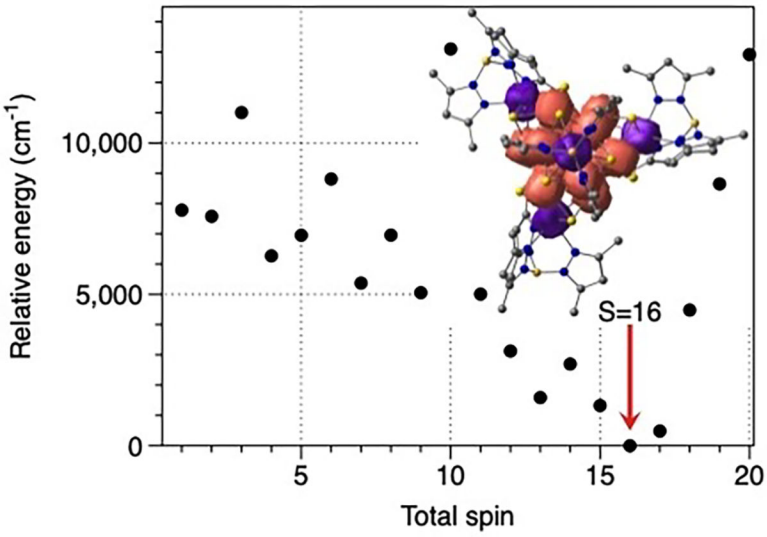

Figure 2.

Relative energies (in cm^{-1}) of spin states from S = 1 to S = 20 of **$Tp^*_4W_4Fe_{13}S_{12}$** complex calculated with BP86/def2-SVP level of theory. Inset: XRD structure of the molecule shown along C_3 symmetry axis with the S = 16 state (lowest energy) spin density iso-surface (contour value 0.008) where positive value shown in coral color and negative value shown in purple color.

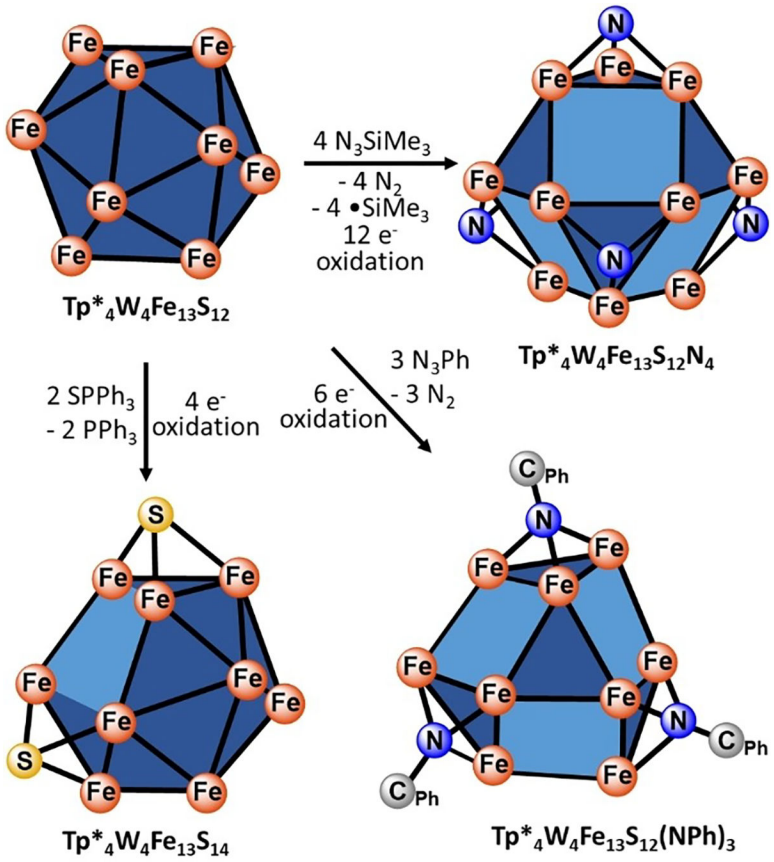

Figure 3.

Reactions of $Tp^*_4W_4Fe_{13}S_{12}$. Tp^*WS_3 fragments are not shown for clarity. Triangular and square faces are shown in dark and light blue, respectively.

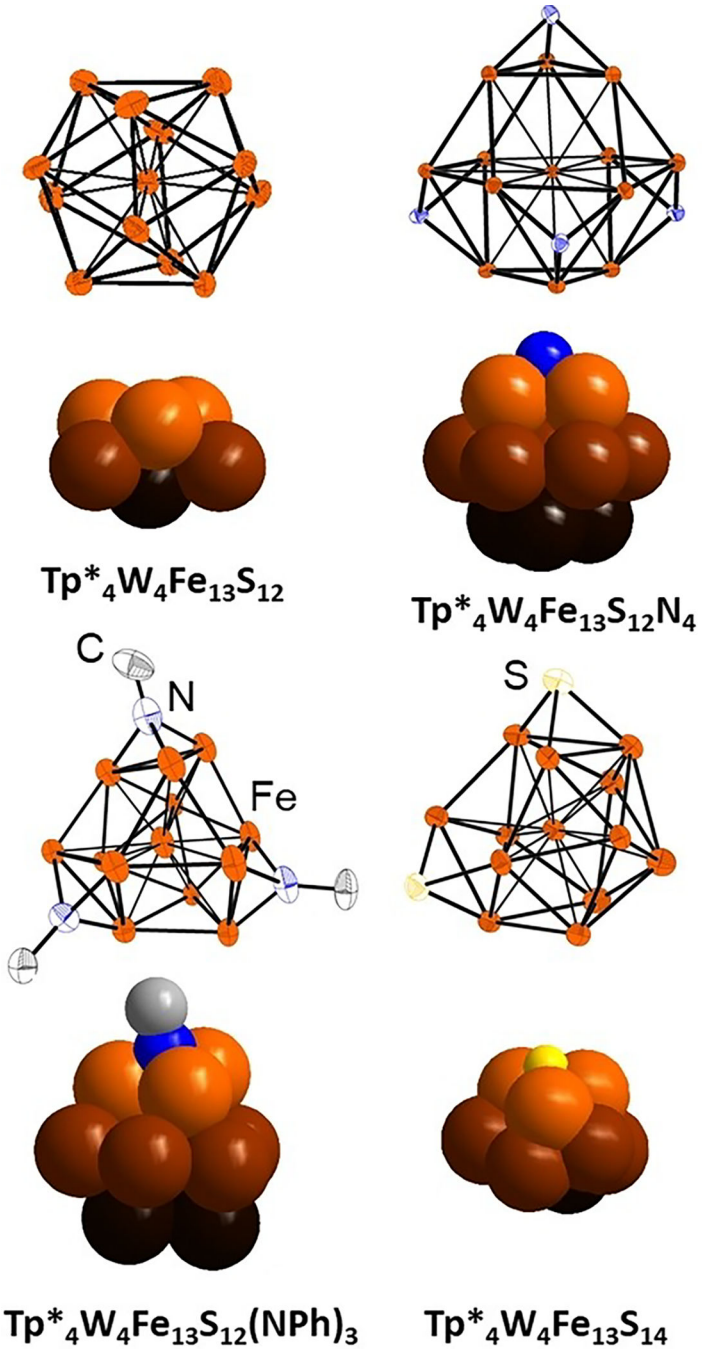

Figure 4.

Thermal ellipsoid plots of Fe_{13} cores with substrate molecules bound for $Tp^*_4W_4Fe_{13}S_{12}$, $Tp^*_4W_4Fe_{13}S_{12}N_4$, $Tp^*_4W_4Fe_{13}S_{12}(NPh)_3$, and $Tp^*_4W_4Fe_{13}S_{14}$ and space filling models for one Fe_3 face of each cluster with one of bound substrate molecules and adjacent Fe atoms shown in different shades of orange based on layer. Ellipsoids are plotted at the 50% probability level.